Applied Physics B (2018) 124:45
https://doi.org/10.1007/s00340-018-6913-1

Applied Physics B
Lasers and Optics

Detecting the propagation effect of terahertz wave inside the two-color femtosecond laser filament in the air

J. Zhao[1] · X. Zhang[2] · S. Li[1] · C. Liu[1] · Y. Chen[1] · Y. Peng[1] · Y. Zhu[1]

Received: 25 October 2017 / Accepted: 9 February 2018

Abstract
In this work, to decide the existence of terahertz (THz) wave propagation effect, THz pulses emitted from a blocked two-color femtosecond laser filament with variable length were recorded by a standard electric–optic sampling setup. The phenomenon of temporal advance of the THz waveform's peak with the increasing filament length has been observed. Together with another method of knife-edge measurement which aims at directly retrieving the THz beam diameter, both the experimental approaches have efficiently indicated the same filament range within which THz wave propagated inside the plasma column. At last, a preliminary two-dimensional near-field scanning imaging of the THz spot inside the cross section of the filament has been suggested as the third way to determine the issue of THz wave propagation effect.

1 Introduction

In the past three decades, terahertz (THz) science and technology has enjoyed a flourishing development [1–3], e.g., in the field of THz source research [4, 5], attracting intense attention from all over the world. Femtosecond laser filamentation is one of the most competitive THz sources for its capability of remotely emitting THz wave with broad bandwidth and high intensity [6, 7]. By simply manipulating the position of a filament, THz pulses can be emitted at a remotely located target, minimizing the strong absorption by water vapor in the atmosphere [8].

Recently, the propagation effect of THz wave along the filament channel has been discovered [9–11]. This effect is mainly associated with the spatial confinement of THz wave inside the filament plasma column, a unique experimental phenomenon that the THz energy is spatially constrained inside a space which is much smaller than the THz wavelength. This new finding could potentially expand THz applications via laser filamentation in various fields, such as remote transmission of THz wave [9], super-resolution THz imaging [10], strong THz electric field for nonlinear optics [11], coherent synthesis enhancement of THz radiation [12], etc.

To detect the presence of THz wave confined propagation during filamentation, two methods have been previously reported [9, 10]. As for single-color photoionization at 800 nm, a Teflon plate was used to block the single-color filament at different longitudinal locations [9]. Temporally advanced THz waveform emitted from longer filament has been observed and proved to be the indicator of THz wave propagation inside the air plasma column. In two-color case (800 + 400 nm), knife-edge (KE) measurements were carried out to directly obtain the THz beam diameter [10]. It has been noticed that, from the beginning towards the middle of the filament, the measured THz beam diameters were much smaller than its wavelength, which is another representative phenomenon of THz wave propagation effect.

In this work, both the above methods have been adopted with the same experimental configuration of two-color laser pumping. First, a ceramic plate was used to cut the two-color filament into different lengths and the emitted THz pulses have been recorded. Second, a printed circuit board (PCB) was applied to scan across the two-color filament, performing KE measurements. At last, a new method has been suggested. A small pinhole was employed as the probe

✉ Y. Peng
py@usst.edu.cn

✉ Y. Zhu
ymzhu@usst.edu.cn

[1] Shanghai Key Laboratory of Modern Optical System, Terahertz Technology Innovation Research Institute, University of Shanghai for Science and Technology, Shanghai 200093, China

[2] Key Laboratory of High Power Laser and Physics, Shanghai Institute of Optics and Fine Mechanics, Chinese Academy of Sciences, Shanghai 201800, China

Published online: 16 February 2018

to perform two-dimensional scanning imaging of the THz spot inside the cross section of the filament.

2 Experimental setup

Figure 1 shows the schematic of our experimental setup, which is a conventional THz time-domain spectroscopy (TDS) system [13–15], consisting of a Ti:sapphire femtosecond laser delivering laser pulses with central wavelength of 800 nm, duration of 50 fs, and energy of 0.45 mJ/pulse at repetition frequency of 1 kHz. Then, the same laser pulse was split into two paths as pump and probe (power ratio 99:1), used for generation and detection of THz wave, respectively. In the pump path, the laser beam was focused by a converging lens ($f = 30$ cm) onto a frequency-doubling crystal (type-I BBO crystal with thickness of 0.1 mm). A two-color laser filament was created at the focus. The exiting THz pulse from the filament was first collimated by an off-axis parabolic mirror ($D = 50$ mm, $f = 100$ mm), and then focused by another identical parabolic mirror onto an electro-optical (EO) crystal (ZnTe crystal with thickness of 1 mm). In addition, a Teflon plate, which has high transmission for THz pulse, was put between the plasma filament and the first off-axis parabolic mirror to block the residual pumping laser. On the other hand, the probe was combined with THz pulse inside the ZnTe crystal by a Pellicle beam splitter, performing electro-optical sampling (EOS) measurement. The detected single-cycle THz pulse had a peak frequency of ~0.4 THz. Next, three different experimental operations have been successively carried out to detect the propagation of THz wave within the two-color filament region, as shown in Fig. 1a–c. Details could be found in the following sections.

3 Experimental operations and results

3.1 Blocking the filament with a ceramic plate

Following [9], a ceramic plate was inserted into the plasma column to terminate the filament, as shown in Fig. 1a. This operation cut the filament into a certain length (from the beginning of the filament to the inserting position of the ceramic plate). Compared with the used Teflon plate adopted in [9], the ceramic plate has better resistance to the ablation of high-intensity femtosecond laser. Besides, THz power transmission for the ceramic plate is acceptable (about 50%). Hence, the THz wave emitted from this length of filament could be efficiently detected by the following EOS setup. It is noteworthy that the above technique might suffer from side effects, such as the intensity-dependent nonlinear refractive index of the blocker (the ceramic plate) caused by its interaction with the intense laser, or the change of the distance between the ZnTe crystal and the THz focus when the ceramic plate was moved. However, these issues have been discussed in detail in our previous report and proved to play a negligible role on the final experimental results [9].

After being inserted, the ceramic plate was moved along the laser propagation direction z in a step length of 0.5 mm, making different lengths of two-color filaments. Meanwhile, the emitted THz pulses are recorded and are presented in Fig. 2a. Noting that z corresponds to the inserting position of the ceramic plate and $z = 0$ is identified as the starting position of the filament, thus, the z value also represents the length of the filament.

Impressively, the temporal location of the maximum of the THz waveforms moved significantly forward with the increasing z. This trend is highlighted in Fig. 2a by a dashed white line which indicates the temporal trajectory of the THz amplitude peak, together with a dashed horizontal line (in

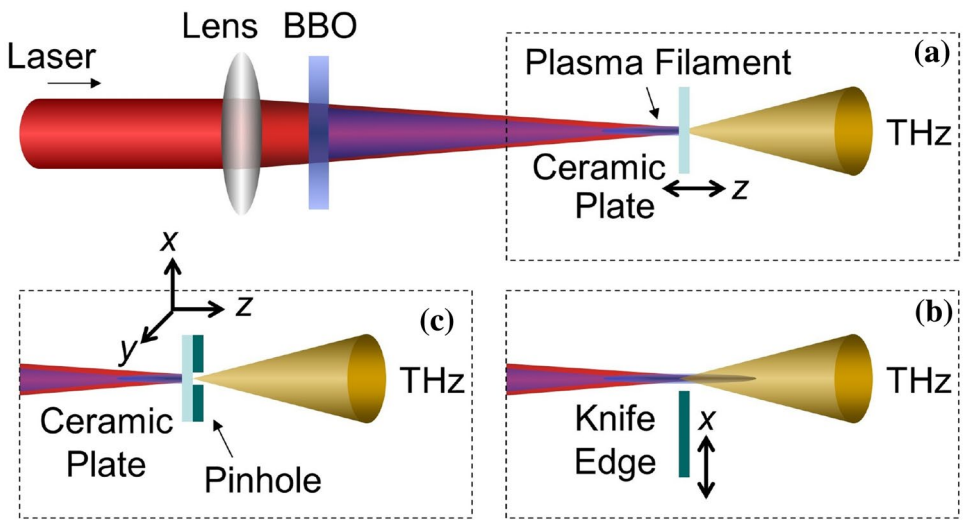

Fig. 1 Schematic of three experimental operations. **a** Ceramic plate was inserted inside the plasma column and moved along z direction. **b** Printed circuit board (PCB) was scanned across the filament along x-axis. **c** Combination of a ceramic plate and an Al pinhole was scanned in the x–y plane inside the plasma filament

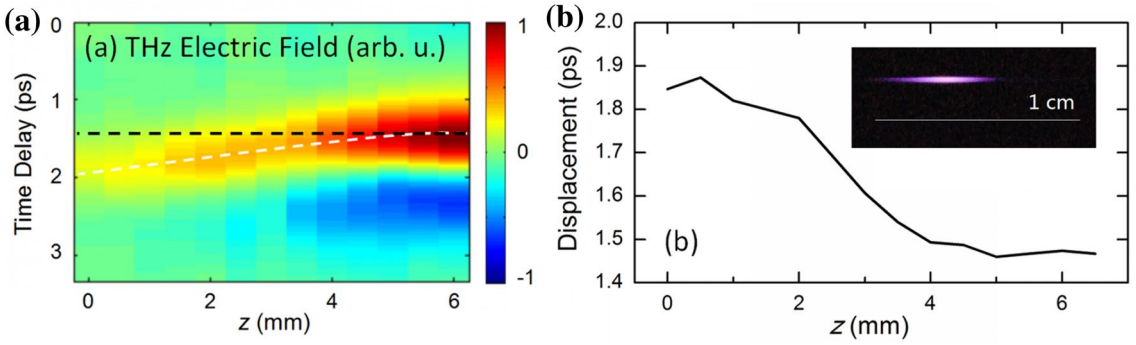

Fig. 2 **a** Recorded THz waveforms as a function of the ceramic plate inserting position z. The dashed white line highlights the temporal advance of the waveform maximum. **b** Displacement evolution of waveform maximum with respect to z. The inset is a side image of the created filament in this work

black) for contrast. Figure 2b further shows the quantified temporal location variation of the THz amplitude maximum, together with a side image of the filament as inset. One can see within the filament zone from $z=0$ to ~5 mm, the temporal advance of waveform maximum existed. Beyond this region, no significant shift of the THz waveform could be observed. The total temporal displacement between waveform maxima at $z=0$ and 5 mm is approximately 0.35 ps.

A number of factors could induce the waveform shift of the detected THz pulse (Fig. 2). One of them could be a gain, which may induce the movement of the pulse envelope maximum (the group velocity of a pulse) [16]. Briefly, when working with a pumped medium, which has a designed gain doublet at two transition frequencies, it is possible to make a pulse propagate with superluminal group velocity but without severe pulse distortion [16]. This is because between the two closely spaced regions of gain, there is steep anomalous dispersion for the frequency components of the pulse, but no strong absorption. In this work, however, no evidence could support the existence of such a exquisite gain doublet in THz band. Moreover, the observed temporal advance mainly comes from the waveform maximum. Thus, we focus on the study of the temporal advance of the maximum of the THz waveform amplitude in the current work, which is also known as superluminal phase velocity of a THz pulse, previously reported by [17, 18].

Furthermore, another possible reason which could induce the THz waveform shift (Fig. 2) might be the conical profile of THz generation front from the filament. However, this could also be excluded, since in our experimental setup, the far-field THz radiation has been collimated and focused onto the ZnTe crystal to be EO detected. This is very different from [7], in which heterodyne detection of THz intensity has been performed at each position of the cross section of the conical THz-emission profile in the far field.

Apart from the above two issues, the recorded waveform shift could be due to the THz refractive index modulation during THz wave propagation within the filament region. In this case, Fourier transformations (FT) on each waveform presented in Fig. 2a have been performed. The resulting phase distributions at different frequencies are shown in Fig. 3a. Along the dashed black line, the phase distribution

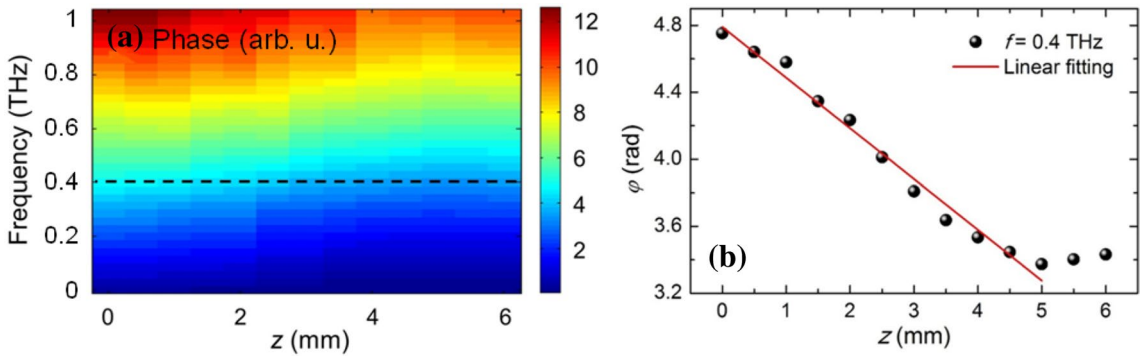

Fig. 3 **a** Phase information at different THz frequencies along z, obtained by Fourier transformations (FT) on the data in Fig. 2a. **b** Representative phase distribution at 0.4 THz with respect to z, extracted along the dashed black line in (**a**). The red line is the corresponding linear fitting result

at 0.4 THz, as an example, is solely illustrated in Fig. 3b as black circles. It can be seen that φ decreased almost linearly between $z=0$–5 mm. Assume that during propagation within the filament region, the refractive index of THz wave is n_{THz}. Hence, the phase variation $d\phi$ in Fig. 3(b) can be written as $d_\varphi = (n_{THz} - n_{THz,air})\cdot(\Omega/c)\cdot dz$, where $n_{THz,air}$ (~ 1.00027 [19]) denote the refractive index of THz wave in the air; c is the light speed in vacuum; Ω is the THz wave angular frequency; and dz indicates the ceramic plate displacement. Thus, n_{THz} could be estimated by the slope of the phase variation curve shown in Fig. 3b between $z=0$ and $z=5$ mm, i.e., $n_{THz} = (c/\Omega)\, d\phi/dz + n_{THz,air}$. The value of the slope ($d\phi$/dz) is given by the linear fitting of $\phi(z)$, as shown as the red line in Fig. 3b.

The calculated n_{THz} at different THz frequencies are shown in Fig. 4a as black circles. The significant discrepancy between the calculated n_{THz} and the reported $n_{THz,air}$ (~ 1.00027 [19], dashed horizontal line in Fig. 4a) implies that the detected THz pulse does not undergo natural diffraction in the air. Furthermore, these n_{THz} values could be explained by the assumption of THz pulse propagating inside the filament plasma. In this case, n_{THz} is the real part of the square root of the permittivity: $n_{THz} = \mathrm{Re}[1 - \omega_p^2/(\omega^2 - i\nu\omega)]^{1/2}$, where ω_p indicates plasma frequency (in SI units): $\omega_p = (e^2 N_e/m_e\varepsilon_0)^{1/2}$. N_e denotes the number density of electrons; e represents the electric charge; m_e indicates the effective mass of the electron; and ε_0 is the permittivity in vacuum. ν corresponds to the typical electron collision frequency inside filament, which is a function of N_e given by Eq. (5) in [20]. Hence, N_e is the only undetermined variable and can be calculated with $n_{THz,}$ as shown in Fig. 4a.

The resulting N_e for each n_{THz} are shown in Fig. 4b, whose values (above 10^{14} cm^{-3}) are much larger than that in the air (N_e~0). This agrees with the above hypothesis of THz wave propagation inside the filament plasma. On the other hand, these N_e values are still quite smaller than the on-axis N_e of the filament which generally is around 10^{16-17} cm^{-3}. This is in accordance with the reported off-axis ring-shaped THz mode field distribution inside the cross section of the filament [10]. Moreover, it can be seen that the calculated N_e increases with the increasing THz frequency (Fig. 4b). This agrees with the fact that higher frequency component of THz wave would be constrained inside the inner ring of the filament, where N_e is larger [10]. Therefore, THz wave could very likely propagate inside the filament ranging from $z=0$ to $z=5$ mm, within which n_{THz} is below the unity (Fig. 4a), and the temporal advance of THz waveforms happened (Fig. 2a).

3.2 Knife-edge (KE) measurement

Next, the THz pulse beam diameters were detected with the same experimental arrangement via KE measurements [10]. In brief, a PCB (opaque for THz wave and femtosecond laser) was used to scan across the filament along x-axis at different z, as shown in Fig. 1b. A representative KE measurement result obtained at $z=9$ mm is displayed as black circles in the inset of Fig. 5. The plot has been normalized to its maximum. Here, a 34.5–93.9% criterion (square root of 11.9–88.1% [21]) has been applied on the detected THz peak-to-peak amplitude, and the corresponding THz beam diameter is $d=0.6$ mm (distance between blue dashed vertical lines in the inset of Fig. 5). All the obtained d as a function of z are depicted, as blue circles in Fig. 5. One can see that, within the region from $z=0$ to $z=5$ mm (shaded area), the THz pulse energy is spatially constrained inside a space with diameter < 40 μm, which is much smaller than the THz wavelength (~ 750 μm at 0.4 THz).

On the other hand, it can be noticed that the confinement region superposes the zone where significant plasma (N_e) was produced during filamentation, as shown as the red line in Fig. 5, which was obtained by a side-imaging approach [22]. Hence, THz wave indeed does undergo spatially confined propagation inside the filament rather than diffraction in the air, mainly in the shaded area ranging from $z=0$ to $z=5$ mm. Moreover, it is noteworthy that the microwave, with even longer wavelength than the THz wave, has also

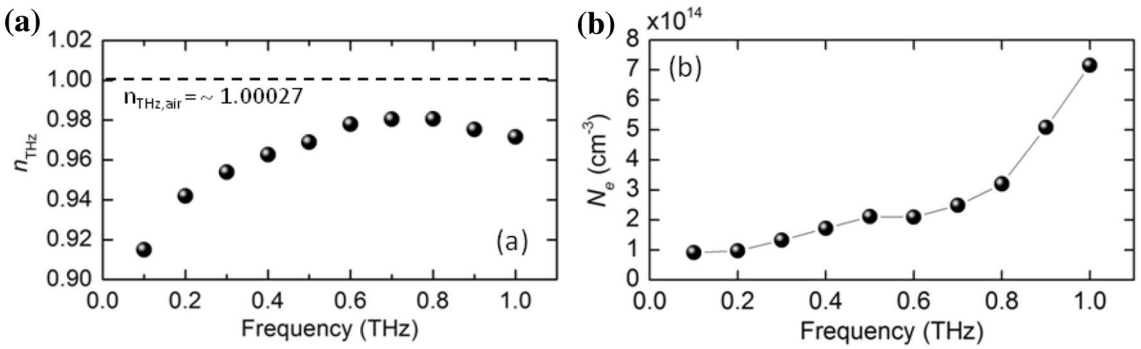

Fig. 4 **a** Experimental THz refractive index n_{THz}. **b** Calculated N_e according to the n_{THz} data in (**a**)

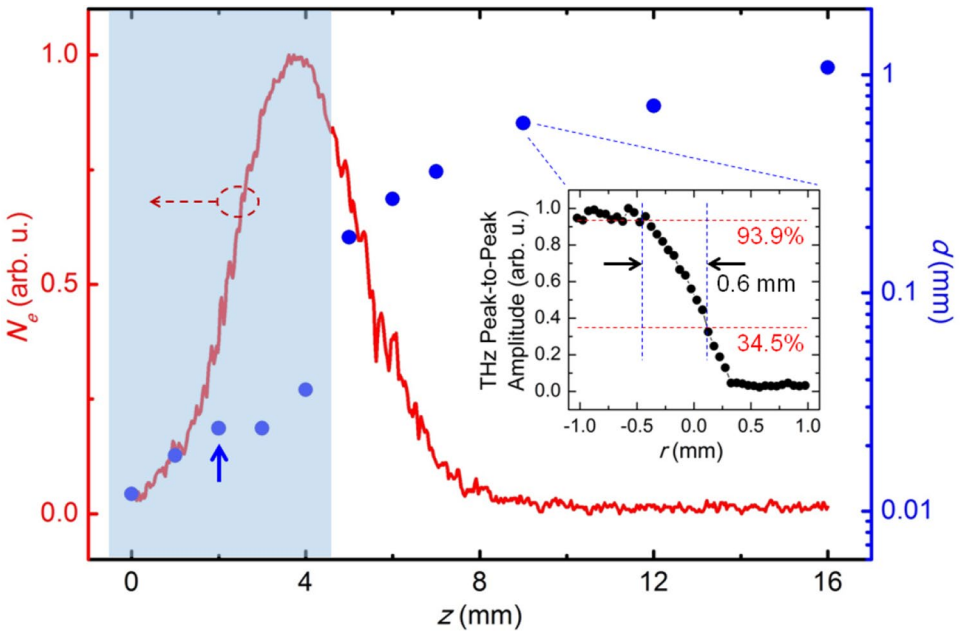

Fig. 5 Evolutions of plasma density N_e (red line) and THz beam diameter d (blue circles) along z. The inset shows a representative KE measurement result at $z = 9$ mm, where 34.5–93.9% criterion has been applied on the recorded THz peak-to-peak amplitude (black solid circles)

been discovered able to be guided along the filament [23, 24].

The aforementioned two methods have both successfully indicated the same filament region (from $z = 0$ to $z = 5$ mm), where THz wave experienced guided propagation. Specifically, the former has indirectly proved this fact by building positive correlation relationship between the experimentally observed THz pulse temporal advance and the assumption of THz propagation inside the plasma (rather than diffraction into air), as well as the resulting refractive index (< 1) in THz band, while the latter has directly demonstrated that by measuring the THz beam diameter inside the cross section of the filament. Compared with each other, the first method of "blocking filament" could be much time-saving, since the second one (KE method) has to repeat the scanning processes along x-axis at different z positions. However, KE measurement offers more valuable information, such as the THz beam diameter. Moreover, it detects the THz beam profile not only within the filament area, but also in the diffraction section after the end of the filament, or even in the far field. Therefore, depending on the demand of either less acquisition time of the signal or more detailed information of interest, one can make a wise choice between these two methods.

3.3 Two-dimensional THz scanning imaging

Besides the above experimental operations and results, actually one may be more interested in the transverse energy distribution pattern of THz beam inside the filament, rather than just the overall diameter (Fig. 5). Hence, a two-dimensional (2-D) near-field THz scanning imaging has been suggested here. This time, an aluminum (Al) pinhole with opening diameter of ~ 10 μm was attached behind the ceramic plate (Fig. 1c). They were fixed together on a two-axis translation stage and inserted into the filament column at $z = \sim 2$ mm (pointed by the upward blue arrow in Fig. 5). Imaging of the THz spot was taken by moving the stage in the x-y plane with step lengths of both 10 μm along x- and y-axes. The ceramic plate terminated the filament and excluded the laser damage of the Al pinhole. Moreover, the Al material is opaque for THz wave. Thus, only the THz energy passing through the pinhole could be detected. In this experimental scheme, a calibrated Golay cell (Tydex) was used for detection, instead of the EOS setup. A 3-THz low-pass filter was positioned in front of the entrance of the Golay cell detector.

The resulting scanning imaging of the THz spot inside the cross section of the filament is displayed in Fig. 6. The overlays in Fig. 6 show the Gaussian fittings for the THz spot sizes in x- and y directions, which are 26 and 21 μm (both FWHM), respectively. These two values basically agree with the KE-measured THz beam diameter of ~ 20 μm inside the filament at $z = 2$ mm, as pointed by the upward arrow (blue) in Fig. 5. It is also worth mentioning that, as for the observed THz spot image, it is a bell-shaped distribution rather than a ring [10]. This is due to the broad detectable bandwidth of the Golay cell detector, which covers THz components from 0.1 to 3 THz (with a low-pass filter), while numerical simulations in [10] have only taken into consideration of THz mode field distribution at mono-frequency.

Compared with the other two methods, the presented near-field THz scanning imaging, without any doubt, is still a preliminary procedure. The opening diameter of the Al pinhole and also the step length of scanning should be

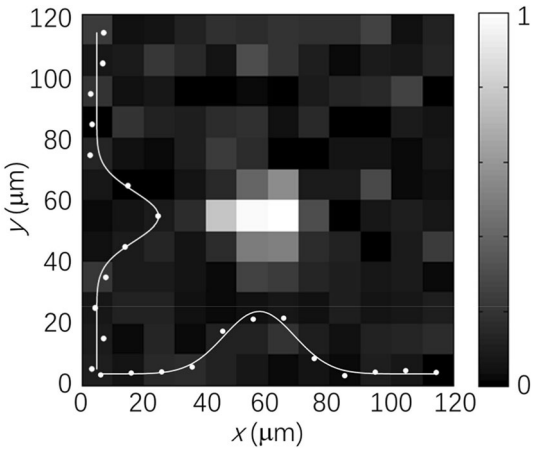

Fig. 6 Two-dimensional scanning image of THz spot inside the cross section of the filament at $z=2$ mm (indicated by the blue upward arrow in Fig. 5). The overlays show THz spot profiles in x and y directions (white circles) and the corresponding Gaussian fittings (white lines)

further decreased (e.g., to 1 μm) to figure out the possible fine structure of energy distribution within the THz spot. Besides, a THz band-pass filter should also be utilized. In this way, one may achieve ring-shaped mode field at a certain THz frequency, verifying the previous simulation outcomes [10]. These studies have been planed and are underway.

4 Discussion

4.1 More choices of the detection schemes

Although the propagation of a THz pulse inside the filament has been demonstrated with three different experimental methods in this work, searching for more evidences is still helpful. As for the method of near-field THz scanning imaging in Sect. 3.3, it would be better if one could substitute the small pinhole, through which little THz energy can be detected, with a THz antenna with microprobe [25]. In this case, the ceramic plate remains stationary, and only the microprobe of the THz detector is 2D scanned on the back surface of the ceramic plate to image the distribution of the transmitted THz electric field.

Furthermore, it has been proved that one is able to observe the filament-guided propagation of a THz pulse, which was injected from another filament, in case of non-collinear two filaments [26]. Inspired by [26], we have planned to inject CW-THz wave from a horn radiator into a filament and detect the filament-guided THz signal. This approach can exclude the interaction between two filaments [26], making the THz pulse propagation inside the filament easy to interpret.

4.2 Underlying mechanisms of the experimental observations

In the above sections, THz wave propagation inside the filament has been experimentally proved. In this section, several theories have been briefly introduced to interpret the underlying physics.

First, in [9], by means of numerical simulations with the commercial software COMSOL, it has been confirmed that the radially non-uniform distribution of the plasma refractive index in THz band could support a THz ring mode within the cross section of the filament. In addition, the maximum THz mode field intensity appears at the vicinity of the refractive index dip, which is similar with the concept of anti-resonance in the field of fiber optics.

Besides, in [11], an analytical model, i.e., one-dimensional negative dielectric optical waveguide (1DND), has been proposed to account for the fact that the detected THz beam diameter is much smaller than the corresponding THz wavelength. The calculated THz electric field has been found to be constrained at the positive–negative dielectric interface of the filament. This time, the THz mode is also in ring-shaped profile, which could be regarded as a kind of surface plasmon wave on the periphery of the filament.

At last, it is well known that the plasma oscillation dominates the THz wave generation process [27]. Moreover, it has been found that a post-process (the so-called "self-action") occurs between the generated THz wave and the plasma (free electrons) [28], during which the THz spectral amplitude and width are modulated. Coincidentally, similar phenomena of THz spectrum modulation could also be observed during THz wave confined propagation along the filament, which has also been attributed to the interaction between the THz wave and the free electrons [29]. Thus, the guided propagation of the THz pulse inside the plasma in this work might be considered as another form of the self-action process, following the plasma oscillation stage during filamentation.

5 Conclusion

In summary, in this work, three methods have been proposed to detect the propagation effect of THz wave inside the two-color femtosecond laser filament. They are (1) inserting a ceramic plate inside the plasma column and moving it along z-axis; (2) scanning a PCB across the filament along x-axis at different z positions; and (3) 2-D scanning imaging the THz spot inside the cross section of the filament. Afterwards, one can decide the existence of constrained THz beam inside the filament according to one of the following experimental observations: temporal advance of THz waveforms, or THz beam diameter being much smaller than its wavelength, or tiny THz spot size within the cross section of the filament. In

the last part of this paper, more detection schemes have been suggested for the future research, which will help reveal the physical nature of the THz wave propagation effect inside the plasma filament.

Acknowledgements National Key R&D Program of China (2017YFC0821300), National Natural Science Foundation of China (11704252, 11574160, 61722111), National Program on Key Basic Research Project of China (973 Program) (2014CB339802, 2014CB339806), the Major National Development Project of Scientific Instrument and Equipment (2017YFF0106300, 2016YFF0100503), the Key Scientific and Technological Project of Science and Technology Commission of Shanghai Municipality (15DZ0500102), Shanghai leading talent (2016-019), and Young Yangtse Rive Scholar (Q2016212).

References

1. A Redo-Sanchez, X.C. Zhang, IEEE J. Sel. Top. Quant. **14**, 260 (2008)
2. M.F. Kimmitt, J. Biol. Phys. **29**, 77 (2003)
3. M.C. Hoffmann, J.A. Fülöp, J. Phys. D Appl. Phys. **44**, 083001 (2011)
4. M. Tonouchi, Nat. Photonics. **1**, 97 (2007)
5. V.L. Bratman, A.G. Litvak, E.V. Suvorov, Phys.-Usp. **54**, 837 (2011)
6. H.G. Roskos, M.D. Thomson, M. Kreß, A.T. Löffler, Laser Photonics Rev. **1**, 349 (2007)
7. C. D'Amico, A. Houard, M. Franco, B. Prade, A. Mysyrowicz, A. Couairon, V.T. Tikhonchuk, Phys. Rev. Lett. **98**, 235002 (2007)
8. T.J. Wang, S. Yuan, Y. Chen, J.F. Daigle, C. Marceau, F. Théberge, M. Châteauneuf, J. Dubois, S.L. Chin, Appl. Phys. Lett. **97**, 111108 (2010)
9. J. Zhao, Y. Zhang, Z. Wang, W. Chu, B. Zeng, W. Liu, Y. Cheng, Z. Xu, Laser Phys. Lett. **11**, 095302 (2014)
10. J. Zhao, W. Chu, L. Guo, Z. Wang, J. Yang, W. Liu, Y. Cheng, Z. Xu, Sci. Rep. **4**, 3880 (2014)
11. J. Zhao, W. Chu, Z. Wang, Y. Peng, C. Gong, L. Lin, Y. Zhu, W. Liu, Y. Cheng, S. Zhuang, Z. Xu, ACS Photonics. **3**, 2338 (2016)
12. J. Zhao, L. Guo, W. Chu, B. Zeng, H. Gao, Y. Cheng, W. Liu, Opt. Lett. **40**, 3838 (2015)
13. Q. Wu, X.C. Zhang, Appl. Phys. Lett. **67**, 3523 (1995)
14. A. Nahata, D.H. Auston, T.F. Heinz, C. Wu, Appl. Phys. Lett. **68**, 150 (1996)
15. P.U. Jepsen, C. Winnewisser, M. Schall, V. Schyja, S.R. Keiding, H. Helm, Phys. Rev. E. **53**, R3052 (1996)
16. L.J. Wang, A. Kuzmich, A. Dogariu, Nature. **406**, 277 (2000)
17. K. Wynne, D.A. Jaroszynski, Opt. Lett. **24**, 25 (1999)
18. J. Lloyd, K. Wang, A. Barkan, D.M. Mittleman, Opt. Commun. **219**, 289 (2003)
19. J. Dai, J. Zhang, W. Zhang, D. Grischkowsky, J. Opt. Soc. Am. B. **21**, 1379 (2004)
20. M. Alshershby, Z. Hao, J. Lin, J. Phys. D: Appl. Phys. **45**, 265401 (2012)
21. A. Dobroiu, M. Yamashita, Y.N. Ohshima, Y. Morita, C. Otani, K. Kawase, Appl. Opt.. **43**, 5637 (2004)
22. S. Xu, X. Sun, B. Zeng, W. Chu, J. Zhao, W. Liu, Y. Cheng, Z. Xu, S.L. Chin, Opt. Express. **20**, 299 (2012)
23. Y. Ren, M. Alshershby, J. Qin, Z. Hao, J. Lin, J. Appl. Phys. **113**, 094904 (2013)
24. M. Alshershby, Y. Ren, J. Qin, Z. Hao, J. Lin, Appl. Phys. Lett. **102**, 204101 (2013)
25. S. Sawallich, B. Globisch, C. Matheisen, M. Nagel, R.J. Dietz, T. Göbel, IEEE T. THz Sci. Techn. **6**, 365 (2016)
26. H.W. Du, H. Hoshina, C. Otani, K. Midorikawa, Appl. Phys. Lett. **107**, 211113 (2015)
27. V.A. Andreeva, O.G. Kosareva, N.A. Panov, D.E. Shipilo, P.M. Solyankin, M.N. Esaulkov, A.P. González de Alaiza Martínez,, V.A. Shkurinov, L. Makarov, S.L. Bergé, Chin, Phys. Rev. Lett. **116**, 063902 (2016)
28. E. Cabrera-Granado, Y. Chen, I. Babushkin, L. Bergé, S. Skupin, New J. Phys. **17**, 023060 (2015)
29. J. Zhao, W. Liu, S. Li, D. Lu, Y. Zhang, Y. Peng, Y. Zhu, S. Zhuang, New clue to thorough understanding terahertz pulse generation by femtosecond laser filamentation Photonics Res. Accepted manuscript (2018)